Simulation of the Geometric Design Parameters' Impact on the Performance of EHD Ion-Drag Micropump

Mohamed Badran
Future University in Egypt (FUE), 90th Street, New Cairo, 11835, Egypt.
mohamed.badran@gmail.com

Abstract: A two-dimensional numerical simulation study has been performed to model an electrohydrodynamic (EHD) micropump. The emphasis of this study was on simulating the effect of the different geometric design parameters on the micropump pressure head and volume flow rate. The simulated design parameters are the channel height, the emitter and collector electrodes heights and widths, and the interelectrode spacing and the spacing between the electrode pairs. The micropump consisted of several electrode pairs which each can be considered as a pumping stage. The simulated working fluid was HFE-7100 3M® thermal fluid. One pumping stage were simulated where the total pressure of the pump can be calculated as pressure of one stage multiplied by the number of stages. The numerical results were first validated with published experimental data then were used to identify the influence of the different design parameters on the pump performance to obtain an optimum design.

Keywords: Electrohydrodynamic, EHD, Ion-Drag, Micropump, Multiphysics COMSOL Simulation, Modeling

Nomenclature

D	Diffusion coefficient (m^2/s)
E_0	Electric charge constant, $1.6x10^{-19}C$
E	Electric field intensity (V/m)
F_e	Electric body force density (N/m^3)
F	Faraday Constant, $96.485x10^3$ (C/mol)
I	Electric current (A)
J	Electric current density (A/m^2)
N_A	Avogadro's number, $6.023x10^{23}$ mol^{-1}
p	Pressure
Q	Fluid flow rate (m^3/s)
u	Velocity of fluid (m/s)
V	Voltage (V)
Greek symbols	
ε	Electric permittivity (F/m)
ε_0	Permittivity of vacuum, $8.854x10^{-12}$ (F/m)
ε_r	Dielectric constant
μ	Dynamic viscosity of fluid (Pa.s)
μ_e	Mobility of charge ($m^2/V.s$)
ρ	Fluid density (kg/m^3)
ρ_e	Volume charge density (C/m^3)
σ	Electric conductivity (S/m)

1. Introduction

Micropumps are crucial in microsystems to generate fluid motion that can be used for pumping, electronics cooling [1], cryogenic cooling [2], agitation or mixing. Their compact sizes and their ability to pump precise volume of fluid make them an attractive candidate for microfluidic systems and biomedical applications [3]. They can be classified as either mechanical or non-mechanical based on how the actuation energy is obtained to drive the fluid.

Some examples of the mechanical micropumps (with moving parts) are electrostatic, piezoelectric, thermopneumatic, and shape memory alloy micropumps. Non-mechanical micropumps (no moving parts) utilize the electric fluid interaction to drive fluid motion such as magnetohydrodynamic, electroosmotic, electrohydrodynamic (EHD), electrochemical micropumps. Nisar et al, presented a review of both the mechanical and non-mechanical micropumps used for biomedical applications [3].

EHD pumping utilizes the influence of an electric field on electric charges, dipoles or particles embedded in a dielectric fluid to move the fluid. Several of the early designs of EHD ion drag pump has been presented in the literature [5-8]. Moreover, the theory of the operation of EHD pumping have been documented in the literature [4, 7-8]. In EHD ion-drag micropump, as shown in Figure 1, an electric field is applied between two sets of electrodes (emitters and collectors) which are in contact with the dielectric fluid. The emitter electrode is where the voltage is applied and the collector electrode is connected to ground. As a result of the high electric field, the emitter electrode will inject electrons into the dielectric

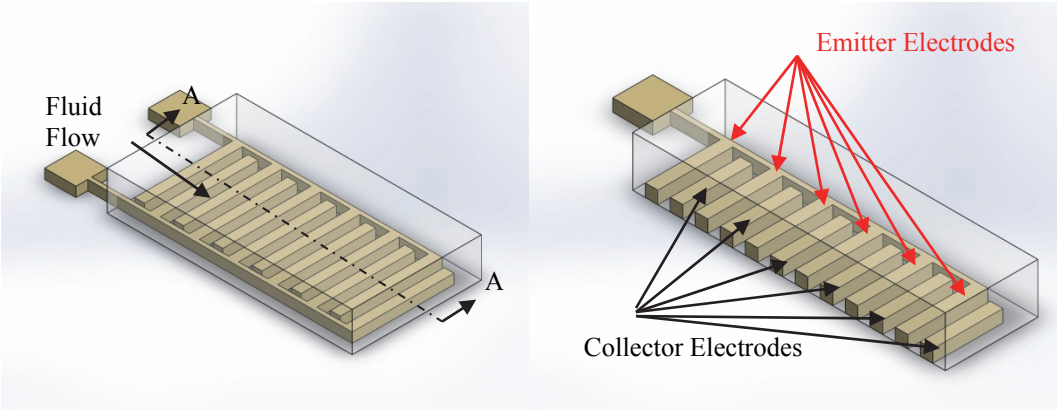

(a) 3-D isometric (b) Section view AA

Figure 1. EHD ion-drag micropump layout

fluid which will ionize the fluid molecules to create ions that will move in the direction of the electric field. This movement will drag the fluid to move in the same direction as the electric field (from the emitter to the collector). A strong electric field will accelerate the ionization process as the electrons of the ionized molecules will be accelerated to ionize other molecules. This will result in increasing the number of ions in the working fluid.

Due to the low conductivity of the dielectric fluid, the current generated due to the high electric field is small which result in low power consumption of the EHD pump.

Since, the pumping action depends on the amount of ions and the ability of the fluid molecules to be ionized, the pumping performance of an EHD ion-drag pump can be increased significantly by the selection of the working fluid properties. Fluids with high permittivity will have higher pumping performance. Moreover, the motion of the fluid depends on the dragging of the working fluid towards the collector. So, working fluids with low viscosity will also increase the pumping performance [9-10].

Several EHD ion-drag micropumps designs had been manufactured and simulated to examine the effects and the influence of the geometric design of the electrodes (height, width, and shape), the interelectrode spacing and the electrode pairs spacing [11-19].

In this study, an extensive parametric modeling of the planar electrode EHD ion-drag micropump was performed. It will examine seven different parameters which are the height of the channel(h_{ch}), height of the emitter(h_e), the height of the collector (h_c), the width of the emitter(w_e), the width of the collector(w_c), the interelectrode spacing(d_{es}), and the electrode pair spacing(d_{ep}). These parameters are shown in Figure 2. Due to the symmetry of the electrode pairs and the absence of variation in the electrodes geometry along the depth, a two dimensional model for only one electrode pair has been used in the study as shown in Figure 2. It has been shown experimentally in different studies that saw tooth geometry of the emitter electrode is better than the planar, as the charge density is higher as the saw tooth tip compared to the planar electrode [14,19]. However, the effect of the other design parameters will affect both designs in the same manner. Therefore, the results of this study will be also applicable to the saw-tooth design.

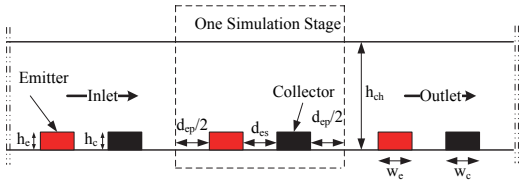

Figure 2. A schematic diagram of the geometric design parameters and the simulation stage

2. Use of COMSOL Multiphysics

2.1 Governing Equations

The driving force for the EHD induced fluid motion is the electric body force. The electric body force density F_e acting on a dielectric fluid with free space charge density ρ_e and subjected to an electric field E is given by equation 1 [20]:

$$F_e = \rho_e E - \frac{1}{2}E^2\nabla\varepsilon + \frac{1}{2}\nabla\left[E^2\rho\left(\frac{\partial\varepsilon}{\partial\rho}\right)_T\right] \quad (1)$$

The electric force density has three components representing different forces acting on the fluid. The first term, called the electrophoretic force, represents the Coulomb force acting on a free space charge. The second term is known as the dielectrophoretic or Kortweg-Helmholtz force density and is defined for two-phase or non-isothermal fluids. The third term is electrostrictive force and is defined for inhomogeneous electric field or fluid compressibility.

Ion-drag pumping uses a single-phase, incompressible fluid placed in a homogenous electric field. Therefore, only Coulomb body force causes mass transport.

The governing equations for ion-drag pumping are the electrical and fluid equations derived from Maxwell's equations, charge and fluid conservation.

Gauss's law, one of Maxwell's equations defines the relationship between the electric field and charge density:

$$\nabla.\vec{E} = \frac{\rho_e}{\varepsilon} \quad (2)$$

In addition, since the magnetic field is negligible,

$$\nabla \times E = 0 \quad (3)$$

The irrotational nature of the electric field yields an expression for the electric field in terms of the potential field gradient.

$$E = -\nabla V \quad (4)$$

The law of conservation of charge states that:

$$\frac{\partial\rho_e}{\partial t} + \nabla.J = 0 \quad (5)$$

where the electric current density, J, is defined as the sum of the current density components both within the control volume medium and due to bulk motion of the medium. So the current density J is:

$$J = \mu_e\rho_e E + D\nabla\rho_e + \rho_e u + \sigma E \quad (6)$$

Under high electric fields, as in ion-drag mechanism, diffusion has a negligible effect compared to the charge migration process and can be ignored. Therefore the current density components become the migration, convection, and conduction respectively. Since we are examining a steady state problem so using both equation 5 and 6, the charge conservation equation becomes:

$$\nabla(\mu_e\rho_e E + \rho_e u + \sigma E) = 0 \quad (7)$$

The electric body force from the electrostatic physics will be combined with the fluidics problem to solve for the velocity and the pressure. Since the fluid flow is assumed to be laminar, steady and an incompressible. The fluid flow is governed by the continuity and Navier-Stokes equations will result into the two equations 8, and 9

$$\nabla.u = 0 \quad (8)$$

$$\rho\left[\frac{\partial u}{\partial t} + (u.\nabla)u\right] = -\nabla p - \mu\nabla^2 u + F_e \quad (9)$$

where $F_e = \rho_e E$

It is required to solve equations 2,4,7,8,and 9 simultaneously for charge density, electric potential, pressure and velocity. Note, that equations 2 and 4 can be combined so the problem is four equations in four unknowns.

2.2 COMSOL modeling

The ion-drag pumping problem can be modeled using three physics which are electrostatics, charge conservation, and laminar flow.

This problem is a fully coupled multiphysics problem. To get the initial value for the electric potential, the electrostatics physics was solved first for the electric potential. Next the electrostatics with the charge conservation were solved together for charge density. Then, the three coupled physics were solved simultaneously for the four unknowns. Note that charge conservation requires the value of the electric potential (migration) and the fluid velocity (convection). In most of the simulations presented in literature, the convection component of the current density were neglected. In this study, this convection

component were modeled through the fully coupled multiphysics.

A parametric two dimensional model was drawn to represent the simulation stage shown in Figure 2. The material for the electrodes was modeled to be gold and the fluid is HFE 7100 3M® thermal fluid.

For electrostatics, the boundary conditions are straight forward, a voltage is applied on the emitter electrode and ground on the collector electrode. A periodic boundary condition is applied on the two ends of the segment as at the midpoint between two adjacent stages, both the geometry and boundary conditions exhibit periodic characteristics.

For the laminar flow, there were two sets of boundary conditions corresponding to the static and dynamic flow conditions. For the static flow condition, where the interest was in the pressure head, the inlet to the stage was modeled at zero pressure while the outlet of the stage was set to no viscus stress. For dynamic flow condition, where the interest was in the velocity or fluid flow rate, the inlet and outlet were modeled at zero pressure. The electric body force density ($\mathbf{F_e} = \boldsymbol{\rho_e}\mathbf{E}$) was modeled as a volume force.

For the charge conservation, there is no physics in COMSOL that can represent the law of conservation of charges. However, the transport of diluted species uses a Nernst-Planck equation for the conservation of concentration of a chemical species as shown in equation 10.

$$\nabla.(-D_i.\nabla c_i - z_i\, \mu_{e,i}\, Fc_i\, \nabla V) + u.\nabla c_i = R_i \qquad (10)$$

This will resemble equation 7, if the concentration is replaced by charge density, and the reaction rate R to be the conductive component in equation 7 ($-\sigma.\nabla E$). Moreover, the diffusion coefficient is set to zero. The charge density will be the concentration multiplied by Avogadro's number (N_A) and the electric charge constant (E_0). The boundary conditions for the charge density are not known. It can be estimated for the measured current during the experiments [15]. The boundary condition will be the charge density at the emitter. A value for the charge density was used from the reported experiments done by Benitis [21].

$\rho_e = \rho_{e,emitter}$ on emitter so that $I_{exp} = \int_A J dA$

2.3 Modeling verification

The model was verified using the experimental data presented in the work of Kazemi et al [19]. Two designs were compared in their work which were symmetric and asymmetric planar electrode designs. The asymmetric dimensions were w_e = 40µm, w_c = 20 µm, h_{ch}=100µm, d_{es}=80µm, d_{ep}=160µm, Number of pairs = 100 and width = 5 mm. The symmetric dimensions were the same except that the w_c=40µm. The reported results were that the micropump volume flow rate (Q, ml/min) and pressure for different emitter voltage.

The model was modified to the experiment dimensions and the velocity was measured at the output in the middle of the outlet cross section. The volume flow rate was evaluated as:
$Q = u.h_{ch}.\text{width}$ (m^3/s) and converted to ml/min. The simulation estimates were in good agreement with the experimental results as shown in Figure 3.

For the same two designs, the pressure was calculated as the differential pressure between outlet and the inlet of the simulation stage and multiplied by the number of stages which was 100 in this case. The simulation estimates were also in good agreement with pressure experimental results of the two designs.

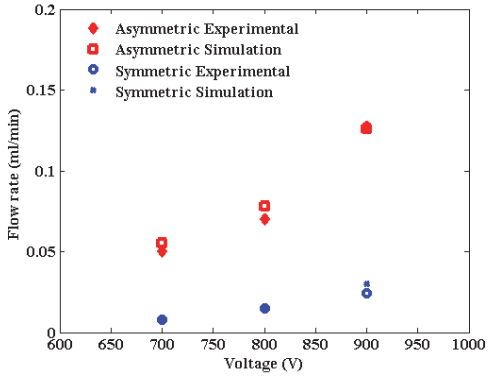

Figure 3. A comparison between Simulated and experimental flow rate

3. Data and Results

In this study, twenty five different designs were simulated to examine the relationship and the influence of the seven aforementioned geometric parameters shown in Figure 2. Three main ratios were introduced which are:

$d_s = d_{ep} / de_s$

$w_r = w_c/w_e$
$h_r = h_c/h_e$

These ratios define the relationship between six of the seven parameters. The last parameter was the channel height which was varied while keeping the other parameters the same.

For the first ratio which was the spacing distance, only the effect of increasing the electrode pair spacing was examined. That is because if both spacing were equal there would be a back flow between the adjacent pairs and no pumping would occur in that design. The impact on both the pressure and volume flow rate were examined as shown in Figure 4. Only the electrode pair spacing was increased while keeping the other parameters constant. As shown in Figure 4, both the flow rate and the pressure per stage increased as the ratio d_s increased. It should be noted that if the width of the pump was limited then as the d_s was increasing the number of stages would decrease. This will result in the decrease of the total pressure.

As shown in Figure 5, a representative pressure contour for the six different designs simulated for this spacing ratio. The pressure was measured as the difference in pressure between the inlet and outlet of the stage.

In Figure 6, the velocity profile of different spacing ratio. It can be shown that velocity was maximum between two electrodes where the maximum electric field. When the spacing ratio increased, the maximum velocity stayed between the electrodes.

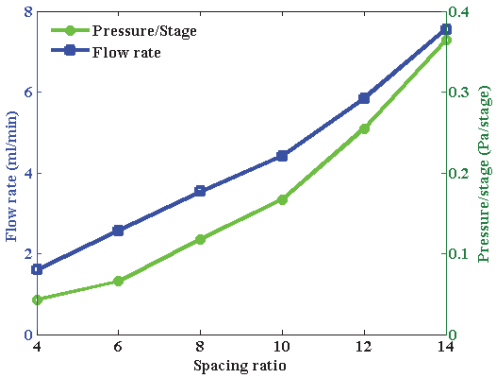

Figure 4. Effects of d_{ep}/d_{es} on the flow rate and the pressure/stage.

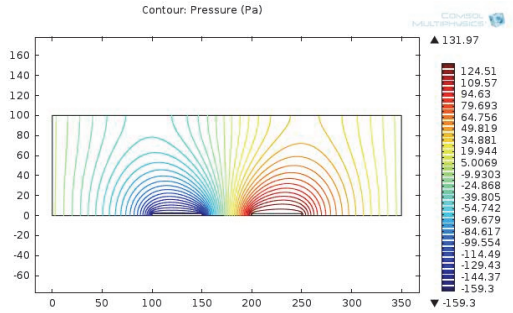

Figure 5. An example of the pressure contour when the $d_s = 4$.

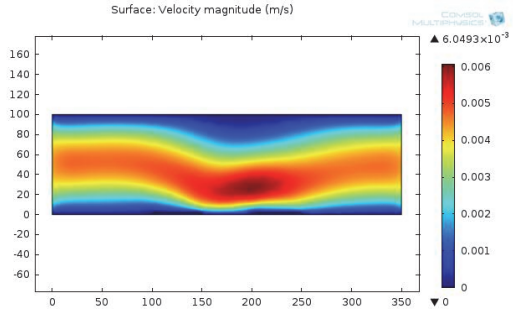

(a) $d_s = 4$

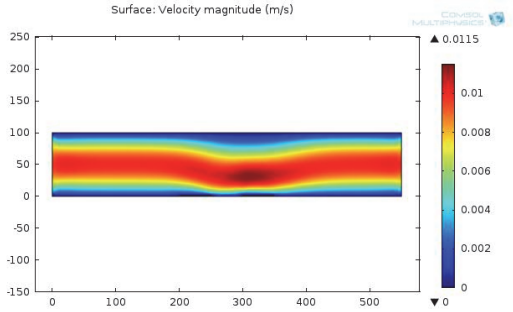

(b) $d_s = 8$

Figure 6. The velocity profile for different d_s ratios

The second ratio was w_r, electrode width ratio. Five designs were studied by varying the w_c and keeping the emitter electrode width constant. As shown in the Figure 7, there is a sharp increase in both the pressure and flow rate when there was asymmetry between the width of the collector and the width of the emitter. However, if the emitter or the collector electrode became too narrow compared to the other electrode, there will be significant back flow between subsequent pair which will affect the pressure and flow rate values. A ratio of two will be optimal and will

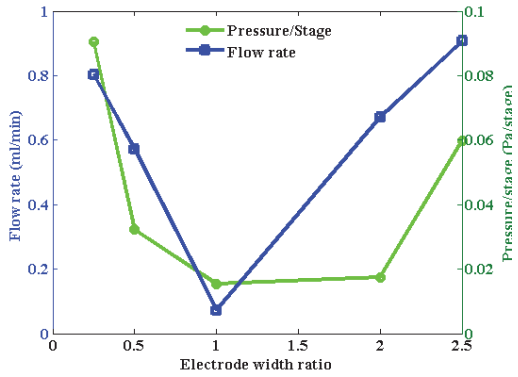

Figure 7. Effects of electrode width ratio on the pump flow rate and pressure/stage.

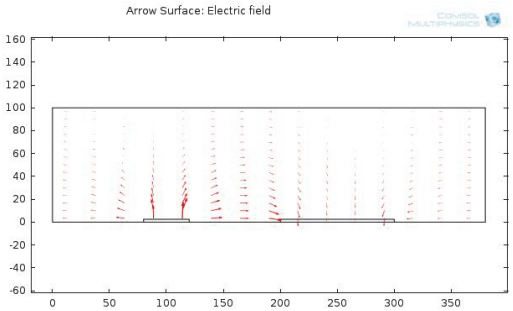

Figure 8. Electric field profile for electrode width ratio of 2.5

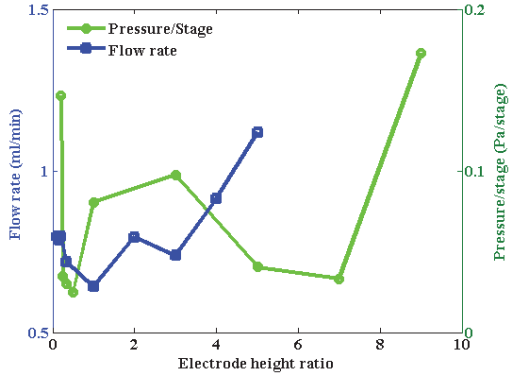

Figure 9. Effects of electrode height ration on the pressure/stage and the flow rate.

minimize the back flow. In Figure 8, a representative of the electric field profile was shown where the field was concentrated between the two electrodes the emitter to the collector.

The last ratio is the electrode height ratio h_r. Nine designs were examined by varying h_e and keeping h_c constant. As shown in Figure 9, the influence of this ratio was that at the extreme cases, the pressure and the flow rate would increase.

The last parameter to be examined is the height of the channel. Five different heights were simulated. It was shown experimentally, that the charge density varies with the height of the channel [21]. For each design, there is a specific height where the charge density reach a plateau at a specific voltage. The value of the charge density varies exponentially with the height. In the simulation, the charge density evaluated in the experiments were used as boundary conditions for the emitter.

As shown in Figure 10, the pressure as well as the flow rate increases with the increase of the height. This due to the fact that as the height increases the charge density increases which will result in a larger electrical body force and consequently faster fluid motion.

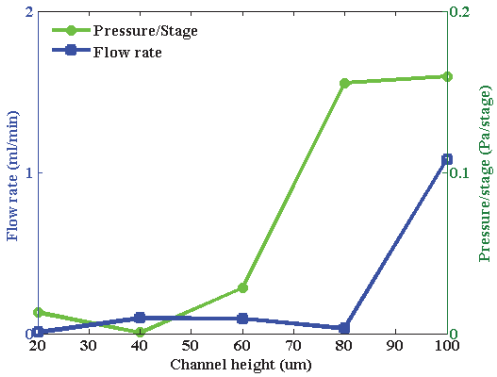

Figure 10. Effect of the channel height on the flow rate and the pressure/stage.

4. Conclusion

In this study, the effects of the different geometric parameters were examined. An optimal design would make use of the asymmetry in width and height between the electrodes. Moreover, the ratio of electrode pair spacing to the interelectrode space should be in the range of 3-4 to benefit from the effect on the pressure and the flow rate and avoid the limitation on the number of electrode pair stages. The height of the channel should be increased up to the point where the charge density reach the plateau. The usage of saw tooth design could be combined with the previously mentioned

features to maximize the gain from the EHD Ion-drag micropump.

5. References

[1] C.K. Lee, A.J. Robinson and C.Y. Ching, "Development of EHD ion-drag micropump for microscale electronics cooling," in *Thermal Investigation of ICs and Systems, 2007. THERMINIC 2007. 13th International Workshop on*, 2007, pp. 48-53.

[2] P. Foroughi, A. Shooshtari, S. Dessiatoun and M.M. Ohadi, "Experimental characterization of an electrohydrodynamic micropump for cryogenic spot cooling applications," *Heat Transfer Eng.*, vol. 31, no. 2, pp. 119-126 2010.

[3] A. Nisar, N. Afzulpurkar, B. Mahaisavariya, and A. Tuantranont, "MEMS-Based micropumps in drug delivery and biomedical applications," *Sensor Actuat. B-Chem.*, vol. 130, pp. 917-942 2008.

[4] W.F. Pickard, "Ion drag pumping. I. theory," *J. Appl. Phys.*, vol. 34, no. 2, pp. 246-250 1963.

[5] W.F. Pickard, "Ion drag pumping. II. experiment," *J. Appl. Phys.*, vol. 34, no. 2, pp. 251-258 1963.

[6] A. Richter and H. Sandmaier, "An electrohydrodynamic micropump," in *Micro Electro Mechanical Systems, 1990. Proceedings, An Investigation of Micro Structures, Sensors, Actuators, Machines and Robots. IEEE*, 1990, pp. 99-104.

[7] O.M. Stuetzer, "Ion drag pumps," *J. Appl. Phys.*, vol. 31, no. 1, pp. 136-146 1960.

[8] O.M. Stuetzer, "Ion drag pressure generation," *J. Appl. Phys.*, vol. 30, no. 7, pp. 984-994 1959.

[9] J.M. Crowley, G.S. Wright and J.C. Chato, "Selecting a working fluid to increase the efficiency and flow rate of an EHD pump," *IEEE Trans. Ind. Appl.*, vol. 26, no. 1, pp. 42-49 1990.

[10] J.E. Bryan and J. Seyed-Yagoobi, "Experimental study of ion-drag pumping using various working fluids," *IEEE Trans. Electr. Insul.*, vol. 26, no. 4, pp. 647-655 1991.

[11] M. Badran and M. Moussa, "On the Design of an Electrohydrodynamic Ion-Drag Micropump," in *MEMS, NANO and Smart Systems, 2004. ICMENS 2004. Proceedings. 2004 International Conference on*, 2004, pp. 137-140.

[12] G. Barbini and G. Coletti, "Influence of electrode geometry on ion-drag pump static pressure," *IEEE Trans. Dielectr. Electr. Insul.*, vol. 2, no. 6, pp. 1100-1105 1995.

[13] J.E. Bryan and J. Seyed-Yagoobi, "An experimental investigation of ion-drag pump in a vertical and axisymmetric configuration," *IEEE Trans. Ind. Appl.*, vol. 28, no. 2, pp. 310-316 1992.

[14] J. Darabi, M. Rada, M. Ohadi and J. Lawler, "Design, fabrication, and testing of an electrohydrodynamic ion-drag micropump," *J. Microelectromech. Syst.*, vol. 11, no. 6, pp. 684-690 2002.

[15] J. Darabi and C. Rhodes, "CFD modeling of an ion-drag micropump," *Sensor Actuat. A-Phys.*, vol. 127, no. 1, pp. 94-103 2006.

[16] S.M. Hasnain, A. Bakshi, P.R. Selvaganapathy and C.Y. Ching, "On the modeling and simulation of ion drag electrohydrodynamic micropumps," *J. Fluids Eng.*, vol. 133, no. 5, pp. 051102 2011.

[17] S.A. Kamboh, J. Labadin and A.R.H. Rigit, "3D Modeling and Simulation of Electrohydrodynamic Ion-Drag Micropump with Different Configurations of Collector Electrode," in *Intelligent Systems, Modelling and Simulation (ISMS), 2012 Third International Conference on*, 2012, pp. 417-422.

[18] P.Z. Kazemi, P.R. Selvaganapathy and C.Y. Ching, "Effect of micropillar electrode spacing on the performance of electrohydrodynamic micropumps," *J. Electrostatics*, vol. 68, no. 4, pp. 376-383 2010.

[19] P.Z. Kazemi, P.R. Selvaganapathy and C.Y. Ching, "Effect of electrode asymmetry on performance of electrohydrodynamic micropumps," *J. Microelectromech. Syst.*, vol. 18; 16, no. 3, pp. 547-554 2009.

[20] A.J. Brad and L.R. Faulkner, *Electrochemical Methods: Fundamentals and Application*, 2nd Edition. John Wiley and Sons, New York, 2001.

[21] V. Benetis, "Experimental and computational investigation of planar ion drag micropump geometrical design parameters," Ph.D dissertation, Univ. Maryland, College Park, MD, 2005.